Tree Physiology 38, 288–302
doi:10.1093/treephys/tpx103

Research paper

X-ray computed microtomography characterizes the wound effect that causes sap flow underestimation by thermal dissipation sensors

S. Marañón-Jiménez[1,7], J. Van den Bulcke[2], A. Piayda[3,4], J. Van Acker[2], M. Cuntz[3,5], C. Rebmann[3] and K. Steppe[6]

[1]University of Granada, Department of Applied Physics, Av. Fuentenueva s/n, 18071 Granada, Spain; [2]UGCT – Woodlab-UGent, Laboratory of Wood Technology, Department of Forest and Water Management, Faculty of Bioscience Engineering, Ghent University, Coupure Links 653, 9000 Gent, Belgium; [3]UFZ, Helmholtz Centre for Environmental Research, Department Computational Hydrosystems, Permoserstraße 15, 04318 Leipzig, Germany; [4]Thünen Institute of Climate-Smart Agriculture, Bundesallee 50, 38116 Braunschweig, Germany; [5]INRA, Université de Lorraine, UMR1137 Ecologie et Ecophysiologie Forestières, 54280 Champenoux, France; [6]Laboratory of Plant Ecology, Department of Applied Ecology and Environmental Biology, Faculty of Bioscience Engineering, Ghent University, Coupure links 653, 9000 Gent, Belgium; [7]Corresponding author (smaranon@ugr.es)

Received May 8, 2017; accepted August 4, 2017; published online September 6, 2017; handling Editor Roberto Tognetti

Insertion of thermal dissipation (TD) sap flow sensors in living tree stems causes damage of the wood tissue, as is the case with other invasive methods. The subsequent wound formation is one of the main causes of underestimation of tree water-use measured by TD sensors. However, the specific alterations in wood anatomy in response to inserted sensors have not yet been characterized, and the linked dysfunctions in xylem conductance and sensor accuracy are still unknown. In this study, we investigate the anatomical mechanisms prompting sap flow underestimation and the dynamic process of wound formation. Successive sets of TD sensors were installed in the early, mid and end stage of the growing season in diffuse- and ring-porous trees, *Fagus sylvatica* (Linnaeus) and *Quercus petraea* ((Mattuschka) Lieblein), respectively. The trees were cut in autumn and additional sensors were installed in the cut stem segments as controls without wound formation. The wounded area and volume surrounding each sensor was then visually determined by X-ray computed microtomography (X-ray microCT). This technique allowed the characterization of vessel anatomical transformations such as tyloses formation, their spatial distribution and quantification of reduction in conductive area. MicroCT scans showed considerable formation of tyloses that reduced the conductive area of vessels surrounding the inserted TD probes, thus causing an underestimation in sap flux density (SFD) in both beech and oak. Discolored wood tissue was ellipsoidal, larger in the radial plane, more extensive in beech than in oak, and also for sensors installed for longer times. However, the severity of anatomical transformations did not always follow this pattern. Increased wound size with time, for example, did not result in larger SFD underestimation. This information helps us to better understand the mechanisms involved in wound effects with TD sensors and allows the provision of practical recommendations to reduce biases associated with wounding in field sap flow measurements.

Keywords: compartmentalization, discoloration, embolism, Granier method, heat transfer, sap velocity, sensor bias, wood anatomy, wound formation.

Introduction

Sap flow sensors are very useful for the assessment of the dynamic response of tree transpiration to changes in environmental variables (i.e., Loustau et al. 1998, Ewers and Oren 2000, Granier et al. 2000, Fiora and Cescatti 2006) but also to obtain absolute estimates of tree transpiration at stand level (Herbst et al. 2007, 2008, Oishi et al. 2010, Clausnitzer et al. 2011, Gebauer et al. 2012, Ringgaard et al. 2012). Most of the sap flux density methods, such as thermal dissipation (TD), heat field deformation (HFD), heat pulse velocity (HPV), Tmax, heat ratio (HR) or Sapflow+, require the insertion of probes within the tree stem (Swanson and Whitfield 1981, Granier 1985, Burgess et al.

2001, Čermák et al. 2004, Davis et al. 2012, Nadezhdina et al. 2012, Vandegehuchte and Steppe 2012, 2013), causing immediate physical damage of the wood tissue and, likely, a subsequent isolating reaction. Several studies suggest that the wound formation may compromise the accuracy of sap flux estimates (Swanson and Whitfield 1981, Smith and Allen 1996, Moore et al. 2010, Steppe et al. 2010, 2015, Wullschleger et al. 2011, Vandegehuchte and Steppe 2013) due to changes in the anatomical and physical properties of the sapwood that surrounds the inserted sensors. The wound effect was nonetheless only widely recognized for the HPV method (Swanson and Whitfield 1981), but recent studies show that the wound effect represents one of the largest sources of underestimation also for the TD method (Wiedemann et al. 2016), which is one of the most widespread sap flow techniques due to low costs and easily comprehensible sensor construction (Davis et al. 2012). However, anatomical mechanisms that cause systematic underestimations of invasive sap flow sensors have barely been assessed, and are unknown for the TD method in particular.

The wood tissue undergoes a series of transformations in response to an injury. More specifically, two phases can be discriminated according to their origin and timing of occurrence. The first phase is the direct and immediate physical damage in the adjacent area to the injury. Insertion of sap flow probes within the sapwood causes such a disturbance of conductive tissues surrounding the measurement point. Vessel rupture, consequent air embolism and interruption of water flow around the drilled holes (Dujesiefken et al. 1999) may cause an unavoidable measurement error inherent to all invasive sap flow sensors (Wullschleger et al. 2011). This error is however accounted for when the method is calibrated under similar conditions. More problematic is the indirect effect, occurring later on, associated with wound reaction close to the damaged area. This reaction was already described by the principle of Compartmentalization Of Damage In Trees (CODIT, Shigo 1984, Liese and Dujesiefken 1996, Dujesiefken et al. 2005). During the healing process, damaged sapwood tissue is actively isolated from healthy tissue by sealing the conductive elements and form components in order to prevent embolism and the spread of pathogens, and to reduce water loss in the surrounding vessels (Shigo 1979). This process is called compartmentalization and the reaction zone surrounding the wound, detectable as a discoloration of sapwood, is characterized by anatomical changes such as tylose formation, thickening of the xylem cell walls, and phenols or gels accumulation (Rioux et al. 1998, Sun et al. 2006). Accumulation of occluding substances can indeed obstruct extensively the conductive vessels in some species (Rioux et al. 1998, De Micco et al. 2016), reducing considerably the conductive capacity of the affected tissue (Dimond 1955). The use of TD sensors to measure sap flow implies not only drilling holes in the stem, but also application of a permanent source of heat in one of the two probes (Granier 1985). Both are causes of disturbance in the wood tissue that can lead to a compartmentalization reaction and subsequent changes in wood anatomy. A reduction of the conductive capacity of vessels and direct changes in wood porosity, composition and density may alter the heat transport in the wood tissue surrounding the inserted probes.

The extent of physical and anatomical transformations of the wounded tissue has been previously linked to a proportional reduction in sensor performance (Barrett et al. 1995, Green et al. 2003, Wullschleger et al. 2011). However, very little is known about the nature of occluding elements, their spatial extension and the temporal dynamics of their development. Wound formation has been observed in response to inserted HPV sensors, where the extension increased with probe thickness and time after installation (Swanson and Whitfield 1981, Barrett et al. 1995, Smith and Allen 1996, Green et al. 2003). The tree wounding reaction is an active defense mechanism of living trees that involves hormone production and biochemical reactions (Shigo 1984). Therefore, a progressive increase in wound size and more severe biochemical and anatomical transformations are expected with time until the damaged tissue is completely compartmentalized (Swanson and Whitfield 1981, Smith and Allen 1996, Sun et al. 2006). Nonetheless, other factors such as tree growth rate, tree age, phenological status, sensor location and climatic conditions can also determine the compartmentalization rate and the extension of wounded wood tissue in response to injuries (Dimond 1955, Shortle et al. 1996, Dujesiefken et al. 1999, 2005, Sun et al. 2006, Moore et al. 2010, Copini et al. 2014*b*). For instance, the compartmentalization reaction is faster and wounds extend less when injuries are formed early in the growing season (Dujesiefken et al. 1999, 2005) at warmer temperatures (Shibata et al. 1981, Moore et al. 2010), in young (Shortle et al. 1996) and fast-growing trees (Dujesiefken et al. 2005) and in the apical part of the trunk (Sun et al. 2006). Analyses of wounded wood tissue in response to other injuries (e.g., boreholes, pruning, insect outbreaks, etc.) have also shown the formation of a compartmentalized area of variable extension and shape according to the size and characteristics of the injury (Dujesiefken et al. 1999, Copini et al. 2014*a*). Nonetheless, spatial and temporal details of wound formation associated with TD sensor installation and use are nonexistent.

Species with different hydraulic architecture may also show contrasting wound reactions (Biggs 1987, Saitoh et al. 1993, Barrett et al. 1995). When sapwood is perforated for sensor installation, air comes into the damaged vessels due to the under-pressure that exists inside. Wider vessels in ring-porous species are more vulnerable to cavitation, pathogens invasion and less efficient in embolism repair compared with diffuse-porous species (Liese and Dujesiefken 1996, Dujesiefken et al. 2005, Moore et al. 2010). The spatial arrangement of vessels in the sapwood will also determine the number of vessels damaged by drilling (Green and Clothier 1988, Dye et al. 1996). In order to prevent pathogen colonization and further embolism in the injured area, irreversibly

caveated vessels undergo a series of anatomical transformations (Zimmermann 1979, Cochard and Tyree 1990, Dujesiefken et al. 1999). Accordingly, more severe wound reactions in response to injuries, evidenced by a higher wound closure, extension of discoloration and soluble phenol content, have been found in oak (ring-porous species) compared with beech (diffuse-porous species) (Dujesiefken et al. 2005). Larger wound extension and more severe anatomical transformations may constitute a key explanatory mechanism for the higher sap flow underestimations reported in ring-porous compared with diffuse-porous species (Green and Clothier 1988, Bush et al. 2010). There are however no precedent studies establishing an empirical relation between wound extension and severity of vessel occlusions and the correspondent species-specific TD sensor bias.

Knowledge on anatomical mechanisms that underlie wound effect underestimation is therefore the next step towards more accurate sap flux estimates with TD and other invasive sap flow sensors. Here, we investigate the anatomical transformations of wood tissue in response to inserted TD probes up to vessel level, and relate these to the reduction in sensor accuracy. Specifically, we determine geometry and extension of the wounded wood tissue according to the time of wounding and application of a constant source of heat in two tree species with different xylem anatomy: ring-porous oak (*Quercus petraea* (Mattuschka) Lieblein) and diffuse-porous beech (*Fagus sylvatica* Linnaeus) trees. Scanning the wounded wood tissues with X-ray computed microtomography (X-ray microCT) also allowed reconstruction of the 3D internal microstructure of the xylem vessels to characterize anatomical transformations occurring inside the conductive vessels. Specifically, the microCT technique provided quantification of the tylose-forming capacity, as proportion of occluded vessels, and the severity of these anomalies, as the proportion of vessel lumen occluded. We hypothesize the formation of larger wounds around sensors that have been inserted for longer times into living stems and in association to heated sensor probes, and more severe anatomical changes in ring-porous trees compared with diffuse-porous trees. We also expect to observe a direct relation between the extension of wound anatomical transformations and bias of the respective sap flow sensor.

Materials and methods

Plant material

Study trees were located in a mixed deciduous forest (Leinefelde, Thüringen, Germany, 51°20′13″N, 10°22′07″E, and 450 m above sea level). Climate in the study area is subatlantic-submontane with an annual mean temperature of 8.2 °C and an annual mean precipitation of 577 mm (2003–14, O. Kolle, Max Planck Institute for Biogeochemistry, Jena, Germany, personal communication). The forest is relatively homogenous and composed by even-aged stands with European beech (*F. sylvatica*) as the dominant species (97% of relative abundance) accompanied by sessile oak (*Q. petraea*, 3%). Tree height and diameter at breast height were 33 m (standard deviation: 7.2 m) and 44 cm (standard deviation: 12.4 cm), respectively (2012, M. Mund, Max Planck Institute for Biogeochemistry, Jena, Germany, personal communication).

Two beech trees (diffuse-porous) and two oak trees (ring-porous) were selected for this experiment so that the anatomical changes associated with wound formation around inserted sap flow sensors could be investigated in two different xylem anatomies. Trees with regular concentric growth, no evidences of knots, scars, diseases or irregularities in the stem surface were chosen.

Thermal dissipation method

The thermal dissipation (TD) sensors were constructed according to Davis et al. (2012) and specifications of the original design of Granier (1985) (see Wiedemann et al. 2016 for further details). Each sensor consisted of two stainless steel needles of 20 mm in length and 1.1 mm in diameter and a T-type thermocouple (copper-constantan). The upper probe of each sensor was continuously heated at constant power (0.2 W) whereas the lower probe measured the ambient temperature of the wood. The constantan ends of the two thermocouples were connected to measure the temperature difference (ΔT) between the probes. The temperature difference was measured every 60 s and the average of 10 min was recorded on a data-logger (CR1000, Campbell Scientific, Logan, UT, USA) and two multiplexers (AM16/32, Campbell Scientific).

ΔT is then related to sap flux density (SFD, $cm^3\,cm^{-2}\,s^{-1}$) using the empirical equation developed by Granier (1985):

$$SFD = 0.0119 * K^{1.231} \quad (1)$$

where 0.0119 and 1.231 are empirically determined coefficients and K is a dimensionless value defined as:

$$K = \frac{\Delta T_0 - \Delta T}{\Delta T} \quad (2)$$

ΔT is the measured temperature difference between the two needles at a given sap flux density. ΔT_0 is the value of ΔT obtained under zero flow conditions or the maximum temperature difference. The custom-built sensors were previously tested against commercially available sensors (Type SF-, Ecomatik, Dachau/Munich, Germany) in order to prove their accuracy and reliability.

Field experimental setup

Six sets of TD sensors were installed at each different date in the growing season (day of year (DOY) 134, 208 and 253; spring, summer and fall sensors, respectively) and in each of the selected trees in the field. Sensors were equally distributed in two 80-cm long stem segments located at two heights (0.9–1.7 m and 2.2–3 m from the base). Hence, each stem height contained three sensors per sampling date located at predefined positions around the stems,

so that each state of wound development would be present along the circumference. A minimal horizontal distance of 20 cm and vertical distance of 40 cm was maintained between consecutive sensors, and vertical alignment was avoided to prevent thermal interference. Stem diameters at sensor positions ranged from 31.4 to 34.1 cm for beech and from 35.3 to 39.2 cm for oak (see Wiedemann et al. 2016 for further details).

For sensor insertion, a small section of the bark was carefully removed and two holes of 2 mm diameter, 2 cm deep and 10 cm apart were drilled radially into the sapwood. A template was used in order to minimize displacement errors during installation. Once the holes were drilled, an aluminum tube of 2 mm diameter with 0.2 mm wall thickness was inserted into each hole so that it was tightly fitted and completely immersed into the sapwood. Sensor probes were then inserted into each corresponding aluminum tube, which was previously filled with silicon grease to increase thermal conductivity. Finally, sensors were protected from physical damages and outdoor conditions and trees were wrapped with aluminum foil to minimize potential natural temperature gradient effects (Do and Rocheteau 2002, Lubczynski et al. 2012).

Trees were logged just before the end of the growing season (DOY 287), i.e., 22, 11 and 5 weeks after installation of spring, summer and fall sensors, respectively. The TD sensors were removed before logging to avoid any damage, while the aluminum tubes remained inserted in the stems. Two 80-cm long sections of each stem, including the aluminum tubes of all installation dates, were cut, wrapped in plastic foil to prevent desiccation and carefully transported to the laboratory.

Laboratory sap flux density measurements with gravimetric reference

Details on the calibration of the TD sensors can be found in Wiedemann et al. (2016). In summary, once in the laboratory, transversal surfaces of stem segments were treated to reopen the blocked vessels and additional TD sensors (i.e., after cutting, AC) were installed following the procedure described above. These measuring points are considered as reference sensor measurements since the wound reaction is an active mechanism of defense that involves hormone production and biochemical reactions (Shigo 1984), so it is not expected to occur in cut stem segments. Existing holes were equipped again with randomly chosen TD sensors in order to avoid any potential sensor bias. Therefore, each segment contained a total of 12 sensors (3 sensors × (3 sampling dates + 1 AC)).

A sap flow calibration test enabled to compare SFD measured by sensors installed in living trees (i.e., with wound compartmentalization reaction: spring, summer, fall sensors) to the freshly installed AC sensors without wound compartmentalization. Constant pressures were applied through the segments, resulting in a SFD of 0 to 25 $cm^3\ cm^{-2}\ h^{-1}$ (gravimetrical reference). This range is within the magnitude reported in the literature (Granier 1985, Steppe et al. 2010) and previously observed in the field by sensor measurements. The gravimetric SFD, considered as reference, was calculated from the rate of change in mass of water collected and normalized for conducting sapwood area (see Wiedemann et al. 2016 for further details).

Wood sample scans

Following the laboratory measurements, a rectangular prism of 3 × 5 × 2 cm (W × H × L) of the wood tissue surrounding the point of insertion of each sensor probe (heated and non-heated probes from each wound age) was cut. Wood sample dimension was chosen a priori based on previous estimations of the extent of wound compartmentalization reaction (Swanson and Whitfield 1981, Sun et al. 2006, Wullschleger et al. 2011). Wood samples were subsequently divided along the longitudinal and tangential axes and the internal radial and transverse surfaces were photographed with a portable scanner (CanoScan LiDE 210 Color Image, Canon, Krefeld, Germany). The extension of discolored area around the probe insertion was quantified with the image-processing software Fiji (Schindelin et al. 2012). Samples were subsequently stored at −18 °C for further analyses.

A subset of six wood samples per species was selected and analyzed by X-ray microCT at the Laboratory of Wood Technology (Woodlab-UGent, Gent, Belgium). One sample of wood tissue adjacent to the heated probes per wound age was randomly chosen, as well as an additional wood sample adjacent to non-heated probes for spring and AC samples. Wood samples were scanned using the multi-resolution X-ray tomography scanner Nanowood (Dierick et al. 2010, 2014). This scanner is custom built at the UGCT (Ghent University Center of Expertise for X-ray Computed Tomography, www.ugct.ugent.be) in collaboration with the company XRE (www.xre.be). Samples were first scanned at 20 μm in both wet and dry conditions (oven-dried samples at 40 °C during 48 h) to determine the volume and shape of the compartmentalized area. Wet samples were most suitable for visualization of the imprint (i.e., marked or delimited area of compartmentalized tissue likely affected by vessel occlusion with tyloses and/or gels) associated with wound formation, although this was only visible in beech X-ray scans (see Results section). Next, the dry wood samples with the oldest wounds (spring) and non-wounded control samples (AC) were scanned at 4 μm resolution for oak and at 1.5 μm resolution for beech. For that, smaller rectangular prisms of 4 × 4 × 6.6 mm (W × H × L) were cut at increasing and consecutive distances from the drilled holes in longitudinal and tangential direction. That allowed characterizing the anatomical transformations caused by probe insertion at the vessel level (Steppe et al. 2004) while enabling a 3D view inside the vessels.

Image processing of X-ray microCT scans

After image acquisition, microCT serial slices (2D transverse cross-sections) of each intact wood sample were virtually reconstructed to a single 3D stack rendering with the software package Octopus 8.7 (Dierick et al. 2004, Vlassenbroeck et al. 2007), licensed by

the spin-off company InsideMatters (www.insidematters.eu). The volume and 3D shape of wounded tissue was determined from the 20 µm 3D stacks of the beech dry wood samples using the Measure Stack plugin (Bob Dougherty, OptiNav Inc.) of the open source image-processing package Fiji (Schindelin et al. 2012). The high-resolution 3D X-ray microCT scans of the wood samples were further analyzed to quantify the proportion of occluded vessels and the reduction in conductive lumen area associated with wound formation. This allowed relating TD sap flow underestimation to the intensity of wood anatomical transformations. The image preparation and analyses were performed with the image-processing package Fiji according to the following workflow steps (Figure 1).

(1) 3D stacks were cropped to exclude irregular margins resulting from the wood sample excision or drilled holes. (2) A Gaussian convolution filter (sigma = 2) was used to smooth the 2D slide images and facilitate vessel edge detection. (3) The 2D slide images were then converted to binary wood-air images by using the iterative IsoData algorithm (auto threshold, Ridler and Calvard 1978). (4) In order to quantify vessels accurately, cracks, crunched tissue in the surrounding of the drill hole and late wood pores were filled using the particle analyzer Biovoxxel Toolbox plugin (Jan Borcher, Biovoxxel, www.biovoxxel.de) by establishing an aspect ratio filter >1 and particle size threshold between 800 and 15,000 pixels for oak and between 400 and 15,000 pixels for beech. (5) Adjacent vessels were then separated using watershed segmentation and their edges smoothed by iteratively minimizing the variance of edge-to-center distance. (6) The convex hull of each vessel was consecutively computed and used to fill remaining vessel edge irregularities. (7) After correct identification of vessels and application of the resulting mask to the original, Gaussian-smoothed image stack, the (x, y) position, area, modal gray value and shape descriptors of each vessel were obtained with the particle analyzer plugin. (8) Next, tyloses were detected by setting an empirical, species-specific threshold according to the deviation of the modal gray value within vessels in each 2D slide, so that lower gray values than this threshold allowed to select the tylose-free vessel area. This modal gray threshold was determined by validating results with the visual identification of tyloses in multiple 2D slide images, and then used for the automated identification of tyloses in all 2D slide images of each 3D stack. Similarly as before, the tylose-free area of each vessel was quantified with the particle analyzer plugin, so that the transverse cross-sectional area of tyloses was calculated as the difference between the total vessel area (step 7) and tylose-free vessel area (step 8). The same procedure was also performed in AC samples in order to account for the residual image noise and for any tyloses that may be naturally present in the wood tissue even without wound reaction. (9) Finally, the area fraction of tyloses within each vessel was calculated as the tylose area over total vessel area. Likewise, the proportion of vessels with tyloses in each 2D slide image was determined.

Statistical analyses

Linear regressions were fitted to the gravimetric sap flux density values and the corresponding sensor records for each date of installation and tree species (see Wiedemann et al. 2016 for further details). The effect of the date of sensor installation and the tree species on the relationship between TD sensor SFD estimates and gravimetrical values were tested using analyses of covariance (ANCOVA) with 'species' or 'date of installation' as fixed factors and the gravimetrical sap flux as the covariate. Data were root-transformed to improve normality and homoscedasticity (Quinn and Keough 2009). Effects of species, date of probe insertion and heat applied to the probes on the extent of discolored area of the wood samples was tested using multifactor ANOVA tests. Likewise, data were previously transformed when required to achieve normality and homoscedasticity. Statistical analyses were performed with JMP Pro 11.0 software (SAS Institute, Cary, NC, USA). Throughout the paper, mean values are followed by ±1 standard error.

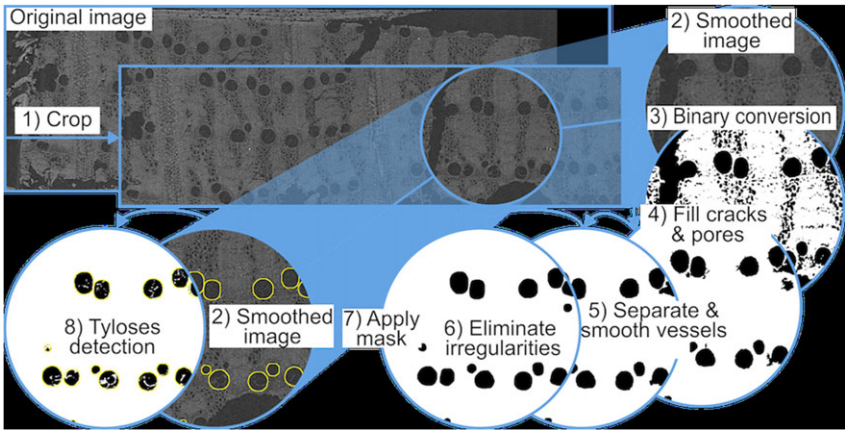

Figure 1. Illustrative scheme on the workflow steps for the image processing of the high-resolution X-ray microCT 3D stacks (4 and 1.5 µm for oak and beech, respectively) to determine the fraction of vessels with tyloses and the transverse cross-sectional area fraction of tyloses within vessels on each 2D image slide.

Results

Discolored wood tissue area

The wood tissue area surrounding the point of sensor insertion showed visual symptoms of wound formation and compartmentalization reaction in both species. This was visible by a clear discoloration of the wounded tissue (Figure 2). This discoloration was clearly visible when the probes were inserted in living trees (spring, summer and fall sensors), but only a discoloration restricted to the area of the drilled hole was visible when sensor installation was done in cut tree stem segments (AC sensors). The extent of discoloration was one order of magnitude larger in the radial than in the transversal plane of the xylem, and more extensive in beech than in oak (Figure 3, Table 1). The discolored areas were also larger in older wounds, as is shown by the larger discolored areas for sensors installed in spring, followed by sensors installed in summer and autumn (Figure 3). Note that the extension of discoloration detected in AC samples corresponds to the area of the drilled holes, exclusively due to the mechanical damage, and not to an active discoloration reaction in the surrounding wood tissue. Heated probes generated a wider discoloration, but the constant heat source did not affect the longitudinal elongation of wounded tissue (Figure 3, Table 1). In addition, there were no significant differences in the extension of the discolored area between the downstream and upstream half of the wood samples, meaning that the wounded area was symmetrical in the radial plane as well as in the transverse plane.

Wood anatomical transformations around the inserted sensors

An elliptical imprint of up to 20 × 29 × 5 mm approx. (longitudinal × radial × tangential) around the inserted probes was clearly visible in beech wood on the 20 μm resolution microCT scans (Figure 4), when the sensors were installed in living trees (i.e., spring, summer and fall wound-affected samples). Imprints were not visible around the sensors installed in cut beech stems (i.e., wound-free AC samples). However, imprints were not visible in any of the oak scans, although tyloses were already visible occluding oak vessels at 20 μm resolution (Figure 5). The imprints in beech were delimited and the compartmentalized volume quantified. The shape was symmetrical in radial and transversal planes (Figure 4) and the volume was larger in older wounds and in wood affected by the heating probes (Figure 6), confirming the visually observed discoloration patterns (Figure 3).

X-ray microCT scans at 4 and 1.5 μm resolution for oak and beech, respectively, allowed us to visualize the anatomical transformations in response to wounding both in oak and beech. When sensors were inserted in living trees, tyloses were formed inside the conductive vessels (Figure 7), interrupting sap flow in the area close to the sensor insertion. Tyloses were not present in vessels of AC wood samples.

Estimation of the span of wood anatomical transformations

The maximum tylose-forming capacity, calculated as the percentage of vessels with tyloses within 1 mm distance from the sensor probe both in the longitudinal and tangential direction was 61.18 ± 8.77% and 64.58 ± 2.75% for spring samples of beech and oak, respectively (Figure 8). This corresponded with a reduction in vessel lumen area of 10.34 ± 1.30% and 8.13 ± 0.30%, respectively. In oak samples, wood anatomical transformations extended more than 20 mm from the point of probe insertion in the longitudinal direction, as was shown by the high and near constant presence of tyloses along the whole length of the scanned sample. However, the presence of tyloses was more restricted in the tangential direction, with a progressive decline up to 15 mm from the point of probe insertion in number of vessels containing tyloses

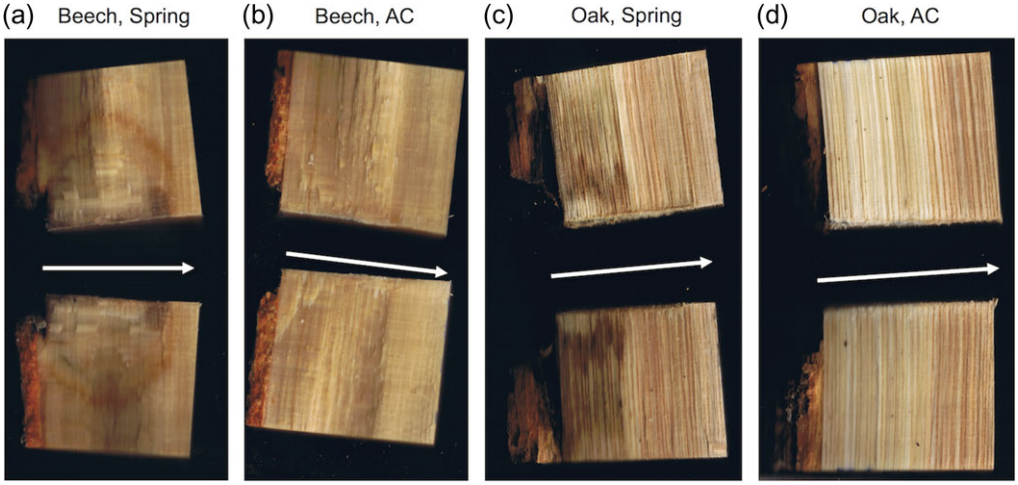

Figure 2. Example of discoloration surrounding the point of probe insertion in beech (a) and oak (c) compared with normal tissue (b and d, respectively). Pictures show the radial plane, the point of sensor insertion is indicated by white arrows; left is the bark. The discolored tissue present in spring samples (a, c) and absent in AC samples (b, d) is an indicator of the compartmentalization reaction.

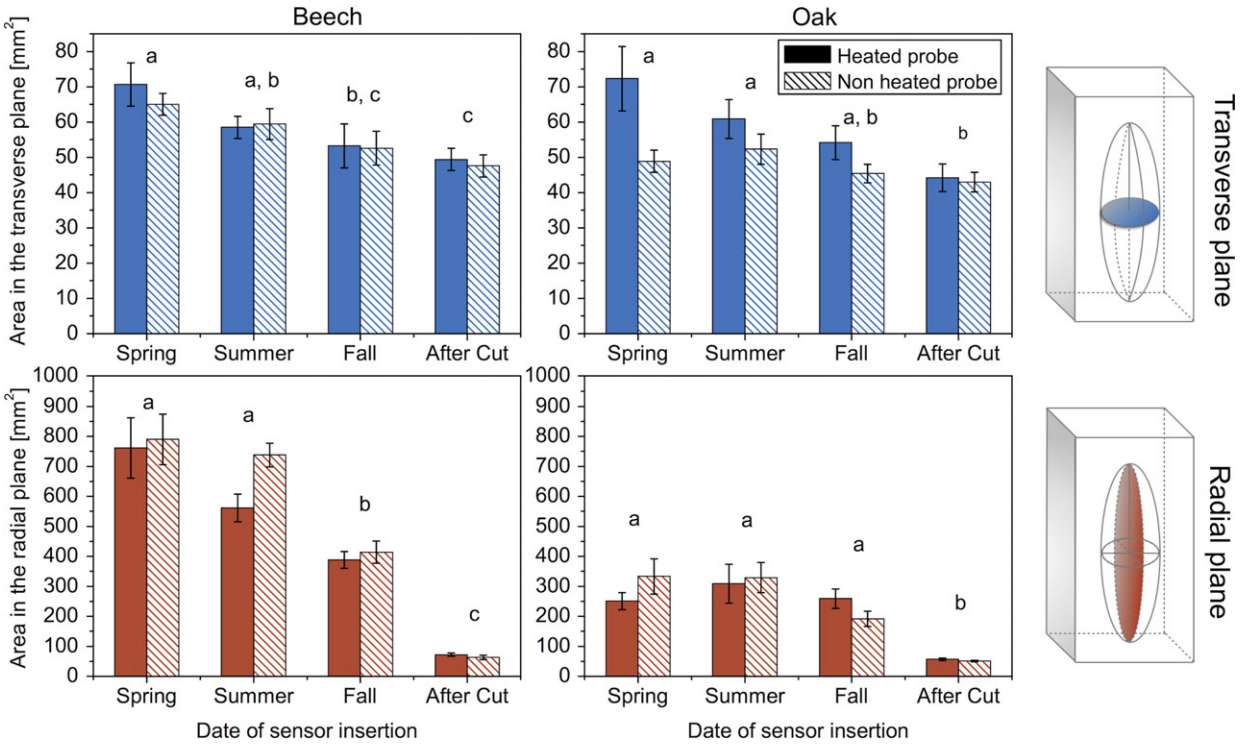

Figure 3. Discolored area in the transverse and the radial plane of the wood samples for beech and oak. Diagrams of the transversal and radial planes of the wood samples are shown at the right hand side of the figure. The *X*-axes indicate the different periods when sensors were installed: Spring, Summer and Fall correspond to sensors installed for 22, 11 and 5 weeks in living stems, respectively. After Cut corresponds to sensors installed in cut tree stems. The effect of applied heat by the heated probes is also shown. Different letters above the bars indicate significant differences among dates (Tukey HSD test after multifactor ANOVA).

Table 1. Results of the ANOVA test of the effects of species, date of the probes insertion and heat applied to the probes on the extension of the discolored area in the radial and transverse sections of the wood tissue. df = degrees of freedom, *F* = values of the statistic, *P* = critical probability, bold values indicate significant effect at $\alpha = 0.05$.

Factor	df	Transversal area (mm^{-2})		Radial area (mm^{-2})	
		F	*P*	*F*	*P*
Species	1	4.74	**0.0309**	99.93	**<0.0001**
Date	3	10.81	**<0.0001**	174.68	**<0.0001**
Heating	1	5.14	**0.0246**	0.07	0.7972
Species × Date	3	0.33	0.8048	7.17	**0.0002**
Species × Heating	1	2.82	0.0951	0.36	0.5487
Date × Heating	3	0.97	0.4093	1.95	0.124
Species × Date × Heating	3	0.55	0.6484	0.57	0.6362

(up to ~10%) and in vessel area covered by tyloses (up to ~3%). In the case of oak, the spatial arrangement of wood anatomical transformations therefore coincided with the elliptical shape of the discoloration (Figure 3). By contrast, in beech samples, the presence of tyloses showed a progressive and similar decline both in the longitudinal and tangential direction from the point of probe insertion, with less than ~20% of vessels with tyloses and ~5% of vessel area covered at a distance of ~8 mm from the probes.

Sap flux density underestimation by thermal dissipation sensors

Freshly installed AC sensors in beech were able to detect the highest proportion of the gravimetric flux (mean of 86.1% ± 5.7%), whereas spring (72.0% ± 4.7%), summer (61.8% ± 3.9%) and fall sensors (58.0% ± 5.0%) underestimated the reference gravimetric SFD values in similar magnitudes (Figure 9a). Differences between AC sensors and sensors installed in living trees (spring, summer and fall) were significant (ANCOVA, $P = 0.0002$). Similar patterns were obtained in the case of oak (Figure 2b), where AC sensors were able to detect a higher (ANCOVA, $P = 0.0015$) proportion of the flux density (72.0% ± 7.8%), compared with spring (40.0% ± 5.1%), summer (52.6% ± 10.5%) and fall sensors (30.8% ± 6.1%). Sensors installed in living trees also showed similar underestimation of the reference gravimetric SFD values (Figure 9b). Nonetheless, only two stem segments could be tested in oak, which explains the lower accuracy also shown by AC sensors, low correlation coefficients with the reference gravimetrical flux density, larger intercepts and higher errors for the linear regression parameters.

Wound-affected sensors showed lower SFD underestimations in beech compared with oak, although differences were statistically marginal and with a significant interaction of species with the gravimetrical flux density (ANCOVA, $P = 0.046$). Wound-free

AC sensors had a similar performance in both beech and oak (ANCOVA, $P = 0.55$) with no significant interactions.

Discussion

Sap flux density measurements are systematically underestimated by sensors that are inserted in living tree stems (Swanson and Whitfield 1981, Steppe et al. 2010, Wiedemann et al. 2016). The wound formation in the living wood tissue that surrounds the inserted sensor probes has been previously suggested as a possible cause. However, hardly any information was available on the anatomical transformations occurring in the conductive sapwood in response to wounding and its impact on the accuracy of SFD estimates. Our results confirm that the damage resulting from drilling holes in living trees to install the TD sensors, and likely any other invasive sap flow sensor, activate the wound compartmentalization reaction. We detected the formation of occluding elements such as tyloses and most likely gels inside the vessels surrounding the inserted probes. The vessel occlusion in this area is unequivocally associated with considerable sap flow underestimations by TD sensors. Characterization of wood anatomical and physiological responses to the inserted sap flow sensors and assessment of their functional significance allowed us to design specific recommendations to improve the accuracy of field SFD estimates.

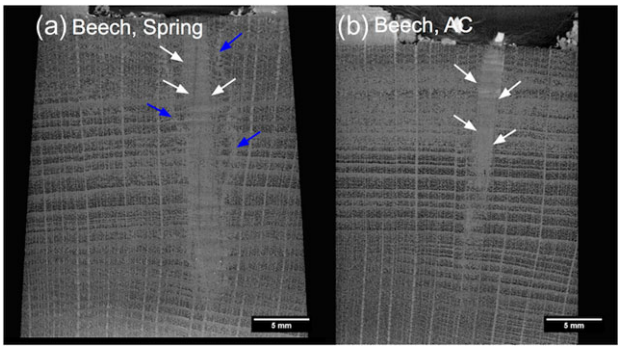

Figure 4. X-ray microCT scans of wood tissue of beech at 20 µm resolution. The images show the transverse cross-section of the wood tissue surrounding probes installed in living trees in spring (a) and in cut stems (AC, b). All images are taken ~2 mm downstream from the probe insertion. The bark is located at the top part of each image. White arrows point at crushed vessels due to mechanical insertion of the probe (in both images), blue arrows in the beech spring sample (a) point at the imprint of the compartmentalized area. This imprint was not visible in AC samples.

Wound-associated anatomical transformations

X-ray microCT scans revealed extensive formation of tyloses inside the conductive vessels adjacent to the inserted sap flow sensors (Figure 7). Tyloses are balloon-like swellings or projections from ray cells, and to a much lesser extent from axial paratracheal parenchyma cells, of xylem that grow into the lumen of adjacent vessels through bordered pits (Zimmermann 1979, Shigo 1991, Pearce 1996, Sun et al. 2008). When vessels are air-filled due to freezing, drought stress or injuries, tyloses intrude from adjacent cells and occlude the vascular tissue to prevent further damage to the plant (Dimond 1955, Aleemullah and Walsh 1996, Parke et al. 2007, Collins et al. 2009, McElrone et al. 2010). Most recent studies point to vessel

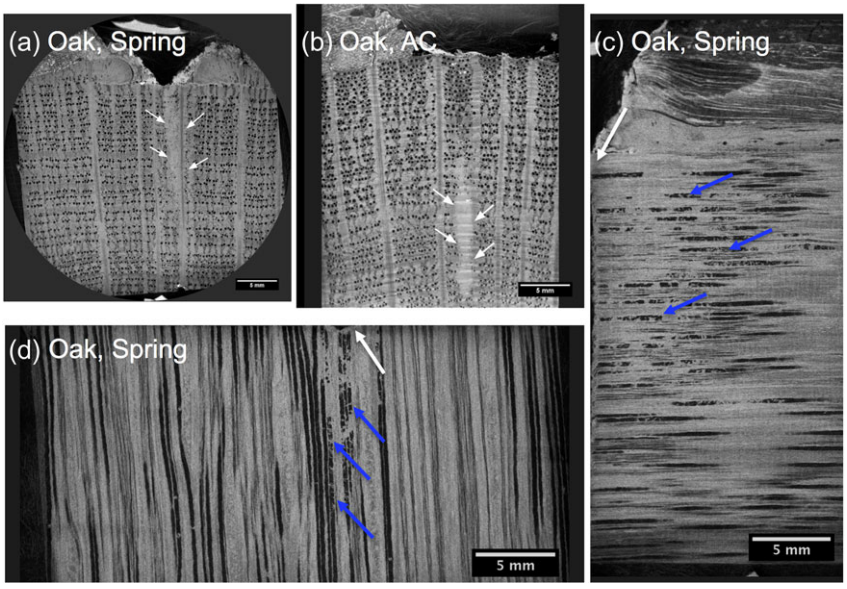

Figure 5. X-ray microCT scans of wood tissue of oak at 20 µm resolution. The images (a) and (b) show the transverse cross-section of the wood tissue surrounding probes installed in living trees in spring (a) and in cut stems (AC, b). The bark is located at the top part of these images. The images (c) and (d) show the radial and tangential sections of the wood tissue surrounding probes installed in living trees in spring. All images are taken ~2 mm downstream from the probe insertion. White arrows point at crushed vessels due to mechanical insertion of the probe or the point of the sensor insertion, blue arrows point to vessels with tyloses.

embolism as a single direct trigger (Rioux et al. 1998, De Micco et al. 2016) despite the fact that the primary stimuli for vessel occlusion in response to injuries is still controversial. Tyloses may, in any case, exert an effective control of pathogen entry from outside and prevent systematic migration (Sun et al. 2006, De Micco et al. 2016).

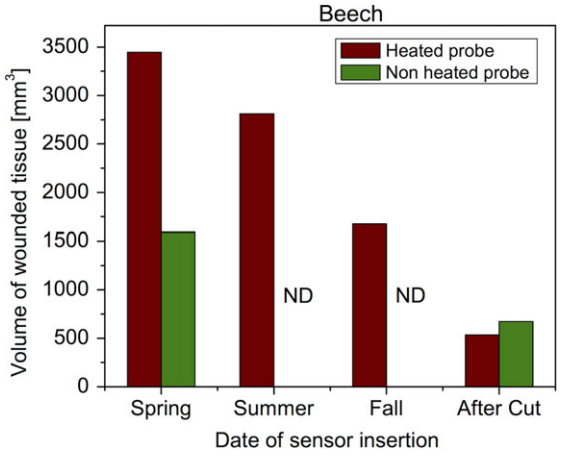

Figure 6. Volume of the compartmentalized area as it was visible on the X-ray microCT scans of beech wood samples at 20 μm resolution. The *X*-axis indicates the different periods when sensors were installed. The effect of the applied heat by the heated probes is also shown.

Tyloses are initially composed by starch and a suberized primary wall layer, which allows tissue impermeabilization by impeding fluid penetration into the vessel (Parameswaran et al. 1985). Once tyloses reach their maximum expansion, they can develop a secondary wall and nucleus, becoming real cells connected to the vessel-associated cells across pits, although nucleus and nucleolus may disappear progressively with age (Zimmermann 1979). At this stage, a multilayered cell wall deposition of suberin or lignification of the tyloses secondary wall can form sclerified tyloses. More specifically, *Fagus* and *Quercus* form suberized tyloses (Schmitt and Liese 1993), which certainly contribute to further constrain water transport (Dimond 1955, Parameswaran et al. 1985, Schmitt and Liese 1993, Parke et al. 2007, Collins et al. 2009).

Other occluding substances can also appear during the compartmentalization reaction in association with tyloses. Increased concentrations of phenols in the compartmentalized tissue act as antibiotics, preventing the pathogens' infection in the area close to the injury (Rioux et al. 1998). Parenchyma cells and tyloses also secrete pectic substances and other polysaccharides (so-called 'gels' (Rioux et al. 1998) or 'gums' in previous literature).

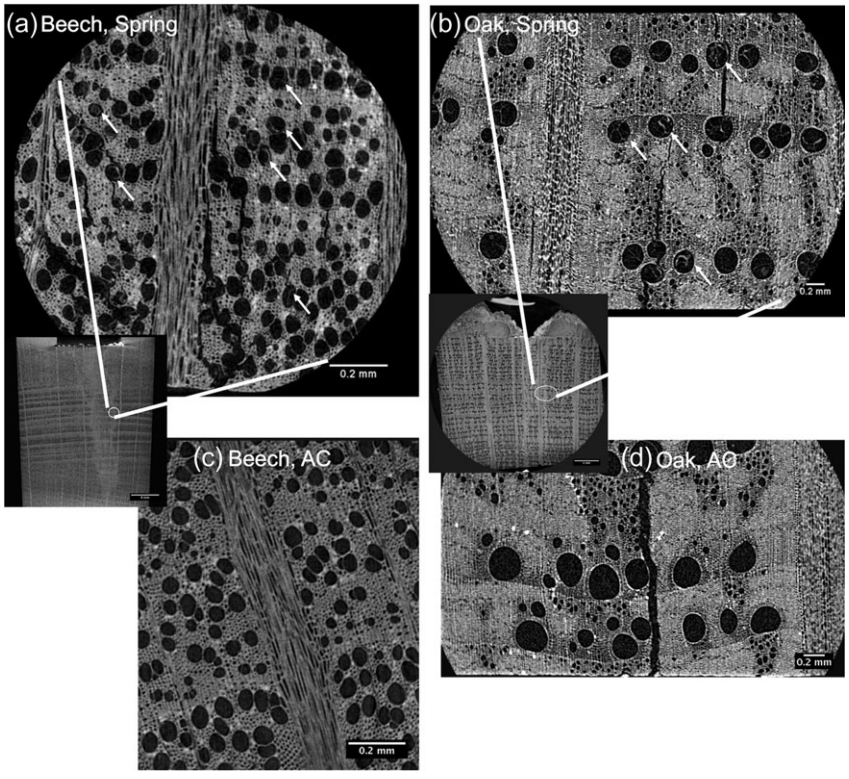

Figure 7. X-ray microCT scans of wood tissue of beech (a, c) and oak (b, d) at 1.5 and 4 μm resolution, respectively. The images are transverse cross-sections of the wood tissue surrounding the probes, which were installed in spring (a, b) and after cutting the stems (AC; c, d). The images were taken ~2 mm downstream from the probe insertion. The approximate location of the images is shown in the corresponding 20 μm scan (small image below the spring samples). White arrows point at tyloses that partially occluded the vessels of the conductive xylem in both species. Tyloses were not observed in AC samples (c, d).

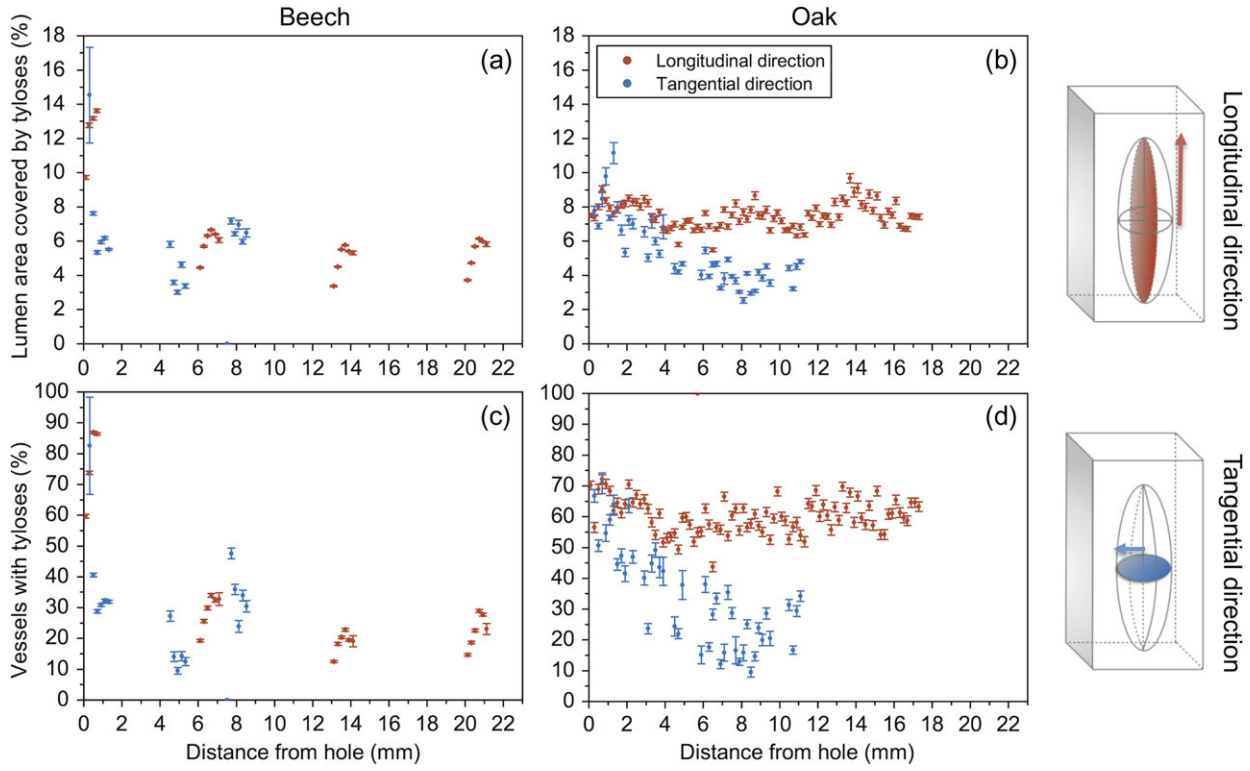

Figure 8. Extent of the anatomical transformations from the point of probe insertion (0 mm from the hole) along the longitudinal and tangential direction of the beech (a, c) and oak (b, d) wood tissue. In (a) and (b) points represent the percentage of vessel lumen area covered by tyloses in each transversal slide. In (c) and (d) each point represents the percentage of vessels partially or totally clogged by tyloses in each transversal slide of the wood sample. Bars represent the standard errors from 50 consecutive slides. Diagrams of the longitudinal and tangential directions of the wood samples are shown at the right. The smallest vessel considered was ca 0.001 mm^2 for beech and 0.01 mm^2 for oak.

Pectin is then dispersed along with the remaining sap movement and it aggregates and swells after impregnation with water still remaining in the vessels. Gels may function as a cement of tyloses and also keep the parenchyma cells adjacent to the occluded vessels hydrated (Rioux et al. 1998). This soluble occluding material that appears early in diseased or injured plants is frequently observed in fresh sections as a translucent and gray area that becomes darker and as solid gum deposit in later wounding stages. Discoloration of living xylem cells may also result from the oxidation of phenols to produce melanoid pigments, which may eventually become trapped in occluding gels in vessels together with dark colored mycelium of fungi infecting the damaged area (Shigo 1979, Dimond 1955, Rioux et al. 1998). Gel expansion in contact with the remaining capillary water may have played a more predominant role in beech vessels due to their smaller size (1909.5 ± 1.9 μm^2 in beech and 45,890 ± 50 μm^2 in oak) and higher density (96.51 ± 0.18 vessels mm^{-2} and 2.794 ± 0.007 vessels mm^{-2}, respectively). This mechanism may actually explain the clear imprints that were visible in microCT scans of wet beech samples (Figure 4) and their absence in oak (Figure 5). Even though these imprints cannot be unequivocally associated to accumulation of gels in this study, the presence of tyloses inside conductive vessels can clearly be distinguished in the microCT scans, which most probably plays a role in the reduction of SFD in the zone around the TD sensors.

Little is known about the formation of tyloses in response to sensor insertion and its implications on measured SFD. Tylose-forming capacity, estimated as the percentage of vessels with tyloses within 20 mm of the drilled hole, was very high in both study species. Up to ~61% and 65% of the conductive vessels were occluded by tyloses within 1 mm distance of the sensor probe both in the longitudinal and tangential directions in beech and oak, respectively (Figure 8c and d). Tylose presence was generalized inside most of the conductive vessels and along a considerable length, but vessel lumen area was only reduced by up to 10% and 8% in beech and oak, respectively (Figure 8a and b). Presence of tyloses thus disturbs considerably the flow path and heat conductivity in the conductive tissue around the sensors, resulting in a significant reduction in sensor accuracy. Actually, the active formation of tyloses in living tree stems, probably together with accumulation of gels that takes place during compartmentalization, caused a 21.4 ± 3% and 47.5 ± 3.8% underestimation in SFD by TD sensors installed in living beech and oak trees, respectively (Figure 9, see Wiedemann et al. 2016 for further details). Nonetheless, differences between

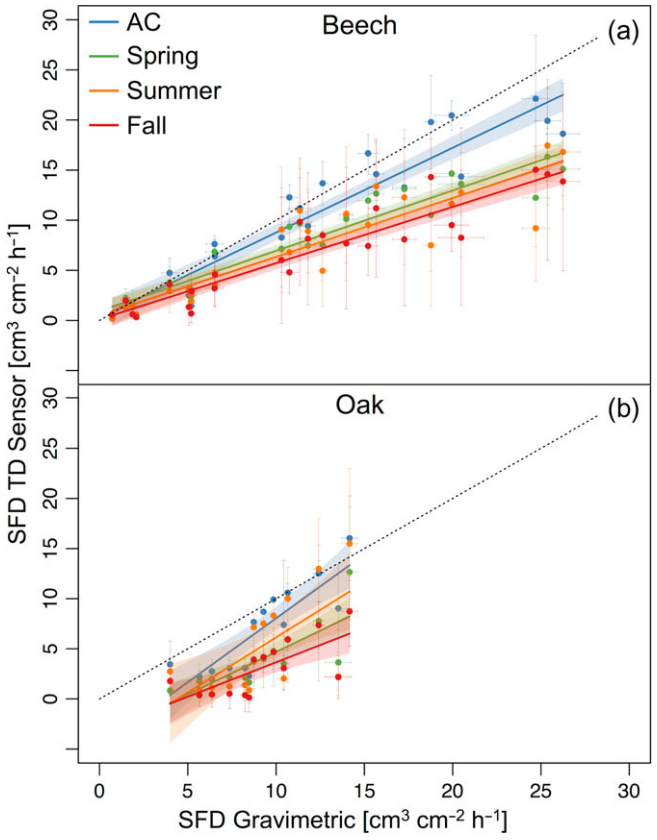

Figure 9. Underestimation of sap flux density by TD sensors determined by lab calibration. Graphs show the comparison of SFD measured by TD sensors and the corresponding gravimetric reference values in (a) beech (*Fagus sylvatica* L., diffuse-porous species) and (b) oak (*Quercus petraea* (Matt.) Liebl., ring-porous species). Markers represent the average values for one calibration step (34–108 sensor readings averaged per data point), including standard errors of the TD sensors and the gravimetric measurements. Solid lines are linear fits while the dashed line is the 1:1 relation. Colored areas represent the 95% confidence intervals of the linear regressions. Redrawn from Wiedemann et al. (2016).

SFD underestimations detected for beech and oak were not statistically significant, neither the tylose-forming capacity and severity of tyloses occlusions within the closest 1 mm from the probes, which impede us from establishing a direct relationship between species-specific differences in wounding reaction and SFD underestimations.

Shape and span of wounded tissue

A clearly visible discolored area surrounded the probes inserted in living trees, whereas discoloration did not occur around the sensors installed in the cut stems (Figure 2). This change in wood color is a clear symptom of wound development in response to an injury (Shigo 1979). The span of discoloration around the probes was one order of magnitude larger in the radial than in the transverse plane (Figure 3) and was symmetrical, resulting in an ellipsoidal area for both species, similar to Barrett et al. (1995). This was consistent with the volume of compartmentalized tissue detected in X-ray microCT scans of beech samples (Figure 4) and with the tylose-forming capacity and severity along the longitudinal and tangential directions in the case of oak (Figure 8b and d). Air bubbles, fungi spores and bacteria can invade vessels damaged by drilling the holes and travel along the conducts along the longitudinal direction. The active sealing of air-filled vessels to prevent the spread of pathogens and/or further embolism (Pearce 1991, Clerivet et al. 2000, Sun et al. 2006, De Micco et al. 2016) resulted in an ellipsoidal compartmentalized area. Likewise, cylindrical increment borers (usually ranging between 4.00 and 5.15 mm diameter) have been reported to also cause wounds that were more extended in the longitudinal direction (length of 16–155 cm) (Dujesiefken et al. 1999). However, wounds generated in response to insertion of cylindrical heat pulse velocity probes have been assumed to be cylindrical in other studies (Swanson and Whitfield 1981, Wullschleger et al. 2011). Since wounds are the result of an active compartmentalization reaction of injured tissue, wound extension will be directly related to the size and shape of these injuries but exacerbated in the sap flow direction, thus resulting in more extended wound reaction in the longitudinal direction.

The span of wounded tissue in the conductive xylem has been previously linked to a direct reduction in sap flow sensor performance (Barrett et al. 1995, Wullschleger et al. 2011). In our study, wound sizes were several orders of magnitude larger than wounds associated with heat pulse probes of similar dimensions: 777 ± 63 mm^2 and 292 ± 33 mm^2 in the radial plane for beech and oak (Figure 3) compared with 4–15 mm^2 reported in Wullschleger et al. (2011), and this was true even for non-heated probes. Wound width also increased in constantly heated TD probes (Figures 3 and 6). In contrast, HPV probes are only heated intermittently during a few seconds. This fact and overlooking the wider extension of wounds in the radial plane and increasing wound sizes with time since HPV probe insertion could partly explain the large differences in wound sizes between these two invasive sap flow methods. Since we did not find a direct relationship between wound extension and the magnitude of SFD underestimations, larger wound sizes in TD sensors can hence not explain completely the larger SFD underestimations compared with other sap flow methods (Steppe et al. 2010).

Our study tree species showed differences between the discoloration extension and anatomical alterations. Discolorations were ellipsoidal in both species but longer in beech samples (Figure 3). On the contrary, tyloses extended similarly in the longitudinal and tangential direction in beech (Figure 8a and c) but more in the longitudinal direction in oak (Figure 8b and d). Therefore, the span of wood anatomical transformations does not necessarily coincide with discolored gel-occluded areas. Pectic material in vessel lumina can actually originate from both the tyloses primary wall (Meyer and Côté 1968, Ouellette 1980, Bonsen and Kučera 1990, Rioux et al. 1998) or directly from the protective layer of xylem parenchyma cells (Bonsen and Kučera 1990, Rioux et al. 1998). Different species may also have divergent mechanisms to ensure

an effective isolation of the damaged tissue by forming prominently either tyloses or gels (Biggs 1987, Bonsen and Kučera 1990, Schmitt and Liese 1990, Saitoh et al. 1993, Rioux et al. 1998, De Micco et al. 2016). Although both oak and beech are tylose and gel-forming species (Von Aufsess 1984, Schwarze and Baum 2000, InsideWood database 2004–onwards, Wheeler 2011), our results suggest that gel production may be more tightly associated to tylose production in oak, where the geometry of discolorations and tyloses coincide. In contrast in beech, parenchyma cells may produce additional pectic material at further distances from the drilled holes to complete the isolation. Despite the fact that no significant differences were detected between SFD underestimations between the two study species (Wiedemann et al. 2016, Figure 9), different wound sizes and wounding mechanisms point to species-dependent wound effects on SFD estimates.

Time frame for wound development

Wounds showed a progressive development up to 22 weeks after sensor insertion in living stems. This is shown by the increasing trend in extension of discolored tissue, particularly in the radial plane (Figure 3, Table 1) and in the volume of compartmentalized area in beech (Figure 6) with the time span of sensor installation in the living tree stem. A faster and more efficient compartmentalization has been described for the early growing season, when physiological mechanisms involved in defense and prevention of pathogen infections are fully active and increased activity of parenchyma cells allow a more efficient formation of accessory substances (Dujesiefken et al. 1999, 2005). Higher temperatures may also facilitate a faster wound reaction, increasing the efficiency of tissue compartmentalization (Shibata et al. 1981, Moore et al. 2010). Production of occluding elements may differ along the year with tyloses forming predominantly in summer and gels in winter (Sun et al. 2008). According to our results, the time span in which sensors have been inserted into the living wood tissue is even more determining for wound size than the tree phenological status or temperature.

Wounds were already present in the autumn wood samples, which were sampled 5 weeks after sensor insertion. This period is consistent with the time span for wound development reported in other studies, e.g., 14–21 days in Smith and Allen (1996), 10–20 days in Swanson and Whitfield (1981) and 7 days after pruning in Sun et al. (2006). We have shown in an earlier study (Wiedemann et al. 2016) that field SFD values decreased immediately after sensor installation and reached stable values after ~2 weeks, which was interpreted as an indication for the time frame of the exhibition of the wound effect symptoms. This time frame should be, nonetheless, considered as a first orientation to demarcate potential wound-affected measurements, since the rate of wound compartmentalization reaction might be influenced by several factors such as tree phenological status, climatic conditions, age, growth rate and sensor location (Liese and Dujesiefken 1996, Shortle et al. 1996, Dujesiefken et al. 1999, 2005, Sun et al. 2006, Moore et al. 2010). To mention some examples, young trees (Shortle et al. 1996), and in general trees with fast growth rates (Dujesiefken et al. 2005), are related to faster injury repair. Tylose development is also much slower in latewood and at the base than in the apical region (Sun et al. 2006). Interestingly, older and larger wounds did not result in larger SFD underestimations by TD sensors (Figure 9). Sensor accuracy may be only sensitive to physical and anatomical transformations in a restricted area close to the sensors. Given the high tylose-forming capacity within the closest millimeters from the sensor probes (Figure 8c and d), even early wounding reactions in this area are sufficient to result in substantial SFD underestimations.

Recommendations to improve the accuracy of the TD method in the field

Most of the sap flow methods require insertion of probes into the living tree stem, which makes them potentially vulnerable to wound-effect bias. This effect is widely recognized for the heat pulse velocity method with specific mathematical corrections available (Swanson and Whitfield 1981). The TD method is, however, based on empirical equations and does not include physical and thermal properties of the wood (Lu et al. 2004), which makes it difficult to implement a correction using a similar approach. Our results suggest that wound development is species-specific, which might translate into species-specific SFD underestimations despite the fact that it could not be detected here (cf. Wiedemann et al. 2016). Many other factors can also influence time and magnitude of the wound effect (Shortle et al. 1996, Dujesiefken et al. 1999, 2005, Moore et al. 2010, Wiedemann et al. 2016), which makes application of a general empirical correction to field sap flux data questionable. A laboratory calibration for each particular case is, on the other hand, very laborious and in most cases not feasible due to logistic reasons or lack of infrastructure (Steppe et al. 2015).

Some preventive measures can be suggested in order to reduce the compartmentalization reaction and tyloses formation near the inserted probes. Drilling the holes carefully at predawn or under overcast meteorological conditions could help to minimize the disruption of the xylem (Lu et al. 2004). A reduced sensor size or the use of chemical inhibitors of tyloses formation (Sun et al. 2007, McElrone et al. 2010) may also contribute to minimize wound-derived bias. Nonetheless, these last two measures may require new calibrations (James et al. 2002) or involve side alterations in hydraulic conductivity, and none of these measures would completely avoid wound formation and hence sap flow underestimation. As is explained in detail in Wiedemann et al. (2016), a field comparison between SFD measured by recently installed sensors, and hence without wound development, and sensors installed in the previous four weeks, hence with developed wounds (Swanson and Whitfield 1981, Smith and Allen 1996), allows determination of the time frame for wound development and, therefore, calculation of a correction for SFD underestimation caused by wound formation. Moreover, similar underestimations regardless the extension of wounds at different stages of development also

imply that wound-derived underestimations are unavoidable 2–4 weeks after sensor installation (Wiedemann et al. 2016). The accuracy of sap flow measurements would be then compromised as soon as wounds start to develop around the inserted probes. The suggested practical approach in Wiedemann et al. (2016) will also offer valuable information about factors influencing the magnitude of the wound effect in each particular case. In the long term, the obtained information could be incorporated into numerical models (Wullschleger et al. 2011), so that specific wound corrections can be developed a priori.

Conclusions

Invasive sap flow sensors can considerably underestimate sap flux density due to wound formation around the probes inserted into living tree stems. X-ray microCT scans allowed us to characterize, for the first time, the anatomical transformations happening in wood tissues and relate them to the corresponding bias of TD sensors. As part of an active compartmentalization reaction, considerable formation of tyloses, and most likely the production of gels, occluded the conductive vessels around the inserted TD probes, which reduced hydraulic conductivity in these areas. The occurrence of tyloses was indeed unequivocally associated with a reduction in detected flow by TD sensors. Tyloses occluded most of the conductive vessels in the zone closest to the sensor, although their spatial distribution did not always coincide with the discolored wound area. Discolorations likely associated with fungi infection and presence of dark colored gels (Dimond 1955, Rioux et al. 1998) were ellipsoidal and larger in the radial plane, and differed between species, with wound age and the presence of a heat source. However, larger wound sizes did not lead to higher SFD underestimations.

Wood anatomical and physiological alterations described here in response to inserted TD sensors may represent one of the main sources of sap flow underestimations in a large proportion of studies worldwide. Wounding occlusions most likely occur in response to any invasive sap flow sensor, since the compartmentalization reaction is common in response to injuries. Moreover, tyloses and other vessel occluding materials have been described in more than 111 and 106 families and subfamilies, respectively, and affect ~17% and 18% of world forests (InsideWood modern wood database 2004–onwards, Wheeler 2011). Both tyloses and solidified gels (gums) in an advanced stage of development, such as the ones present in discolored wound tissues, can be considered as irreversible vessel occlusions, since they would require very complex processes to be degraded (De Micco et al. 2016). Despite its relevance, the use of a universal wound correction factor is probably not advisable (Wiedemann et al. 2016), since the formation of occluding elements is influenced by wound age, tree species and the presence of a heat source as well as by climatic conditions, sensor dimensions and phenology, amongst others. The information provided in our study contributes to the ability to detect potential biased sap flow measurements a priori and to design strategies to improve the accuracy of invasive techniques.

Acknowledgments

We thank the members of the field-research groups of the Max Planck Institute for Biogeochemistry, Jena, the Chair of Bioclimatology of the University of Göttingen and the forestry office of Leinefelde for their support with cutting the trees. Special thanks goes to all members of the field-research group of the UFZ Department Computational Hydrosystems for their support during field and lab experiments, in particular to Andreas Wiedemann, Sebastian Gimper, Hendrik Zöphel, Laura Dienstbach and Inmaculada García Quirós.

Conflict of interest

None declared.

Funding

Project supported by the European Union Seventh Framework Programme – 'Trees4Future' – (284181 to SM-J), by the European Union's Seventh Framework Program Marie Skłodowska-Curie actions and the Ministry of Economy, Innovation, Science and Employment of the Junta de Andalucía – 'Andalucía Talent Hub Program' – (COFUND – Grant agreement 291780 to SM-J), by the Spanish Ministry of Economy and Competitiveness, including European Regional Development Funds – 'GEISpain' – (CGL2014-52838-C2-1-R), and by the German Federal Ministry of Education and Research – 'INFLUINS' (03 IS 2001 A).

References

Aleemullah M, Walsh KB (1996) Australian papaya dieback: evidence against the calcium deficiency hypothesis and observations on the significance of laticifer autofluorescence. Aust J Agric Res 47:371–385.

Barrett DJ, Hatton TJ, Ash JE, Ball MC (1995) Evaluation of the heat pulse velocity technique for measurement of sap flow in rainforest and eucalypt forest species of south-eastern Australia. Plant Cell Environ 18: 463–469.

Biggs AR (1987) Occurrence and location of tuberin in wound reaction zones in xylem of 17 tree species. Phytopathology 77:718–725.

Bonsen KJM, Kučera LJ (1990) Vessel occlusions in plants: morphological function and evolutionary aspects. IAWA Bull 11:393–399.

Burgess SSO, Adams MA, Turner NC, Beverly CR, Ong CK, Khan AAH, Bleby TM (2001) An improved heat pulse method to measure low and reverse rates of sap flow in woody plants. Tree Physiol 21: 589–598.

Bush SE, Hultine KR, Sperry JS, Ehleringer JR (2010) Calibration of thermal dissipation sap flow probes for ring- and diffuse-porous trees. Tree Physiol 30:1545–1554.

Čermák J, Kučera J, Nadezhdina N (2004) Sap flow measurements with some thermodynamic methods, flow integration within trees and scaling up from sample trees to entire forest stands. Trees Struct Funct 18:529–546.

Clausnitzer F, Köstner B, Schwärzel K (2011) Relationships between canopy transpiration, atmospheric conditions and soil water availability – analyses of long-term sap-flow measurements in an old Norway spruce forest at the Ore Mountains/Germany. Agric For Meteorol 151: 1023–1034.

Clerivet A, Déon V, Alami I, Lopez F, Geiger JP, Nicole M (2000) Tyloses and gels associated with cellulose accumulation in vessels are responses of plane tree seedlings (*Platanus* × *acerifolia*) to the vascular fungus *Ceratocystis fimbriata* f. sp. *platani*. Trees 15:25–31.

Cochard H, Tyree MT (1990) Xylem dysfunction in *Quercus*: vessel sizes, tyloses, cavitation and seasonal changes in embolism. Tree Physiol 6:393–407.

Collins BR, Parke JL, Lachenbruch B, Hansen EM (2009) The effects of *Phytophthora ramorum* infection on the hydraulic conductivity and tylosis formation in tanoak sapwood. Can J For Res 39:1766–1776.

Copini P, den Ouden J, Decuyper M, Mohren GMJ, Loomans AJM, Sass-Klaassen U (2014*a*) Early wound reactions of Japanese maple during winter dormancy: the effect of two contrasting temperature regimes. AoB Plants 6:plu059.

Copini P, Sass-Klaassen U, Ouden DJ (2014*b*) Precision of dating insect outbreaks using wood anatomy: the case of *Anoplophora* in Japanese maple. Trees 28:103–113.

Davis TW, Kuo C-M, Liang X, Yu P-S (2012) Sap flow sensors: construction, quality control and comparison. Sensors 12:954–971.

De Micco V, Balzano A, Wheeler EA, Baas P (2016) Tyloses and gums: a review of structure, function and occurrence of vessel occlusions. IAWA J 37:186–205.

Dierick M, Masschaele B, Van Hoorebeke L (2004) Octopus, a fast and user-friendly tomographic reconstruction package developed in LabView®. Meas Sci Technol 15:1366–1370.

Dierick M, Loo VD, Masschaele B (2010) A LabVIEW® based generic CT scanner control software platform. J Xray Sci Technol 18:451–461.

Dierick M, Loo VD, Masschaele B (2014) Recent micro-CT scanner developments at UGCT. Nucl Instrum Methods Phys Res B 324:35–40.

Dimond AE (1955) Pathogenesis in the wilt diseases. Annu Rev Plant Physiol 6:329–350.

Do F, Rocheteau A (2002) Influence of natural temperature gradients on measurements of xylem sap flow with thermal dissipation probes. 2. Advantages and calibration of a noncontinuous heating system. Tree Physiol 22:649–654.

Dujesiefken D, Rhaesa A, Eckstein D, Stobbe H (1999) Tree wound reaction of differently treated boreholes. J Arboric 25:113–123.

Dujesiefken D, Liese W, Shortle W, Minocha R (2005) Response of beech and oaks to wounds made at different times of the year. Eur J For Res 124:113–117.

Dye PJ, Soko S, Poulter AG (1996) Evaluation of the heat pulse velocity method for measuring sap flow in *Pinus patula*. J Exp Bot 47:975–981.

Ewers BE, Oren R (2000) Analyses of assumptions and errors in the calculation of stomatal conductance from sap flux measurements. Tree Physiol 20:579–589.

Fiora A, Cescatti A (2006) Diurnal and seasonal variability in radial distribution of sap flux density: implications for estimating stand transpiration. Tree Physiol 26:1217–1225.

Gebauer T, Horna V, Leuschner C (2012) Canopy transpiration of pure and mixed forest stands with variable abundance of European beech. J Hydrol 442–443:2–14.

Granier A (1985) A new method of sap flow measurement in tree stems. Ann Sci For 42:193–200.

Granier A, Biron P, Lemoine D (2000) Water balance, transpiration and canopy conductance in two beech stands. Agric For Meteorol 100: 291–308.

Green S, Clothier B, Jardine B (2003) Theory and practical application of heat pulse to measure sap flow. Agron J 95:1371–1379.

Green SR, Clothier BE (1988) Water use of kiwifruit vines and apple trees by the heat-pulse technique. J Exp Bot 39:115–123.

Herbst M, Roberts JM, Rosier PTW, Taylor ME, Gowing DJ (2007) Edge effects and forest water use: a field study in a mixed deciduous woodland. For Ecol Manage 250:176–186.

Herbst M, Rosier PTW, Morecroft MD, Gowing DJ (2008) Comparative measurements of transpiration and canopy conductance in two mixed deciduous woodlands differing in structure and species composition. Tree Physiol 28:959–970.

James SA, Clearwater MJ, Meinzer FC, Goldstein G (2002) Heat dissipation sensors of variable length for the measurement of sap flow in trees with deep sapwood. Tree Physiol 22:277–283.

Liese W, Dujesiefken D (1996) Wound reactions of trees. In: Raychaudhuri SP, Maramosch K (eds) Forest trees and palms – disease and control. Oxford and IBH Publishing Co PVT LTD, New Delhi, India, pp 20–42.

Loustau D, Domec JC, Bosc A (1998) Interpreting the variations in xylem sap flux density within the trunk of maritime pine (*Pinus pinaster* Ait.): application of a model for calculating water flows at tree and stand levels. Ann For Sci 55:29–46.

Lu P, Urban L, Zhao P (2004) Granier's thermal dissipation probe (TDP) method for measuring sap flow in trees: theory and practice. Acta Bot Sinica 46:631–646.

Lubczynski MW, Chavarro-Rincon D, Roy J (2012) Novel, cyclic heat dissipation method for the correction of natural temperature gradients in sap flow measurements. Part 1. Theory and application. Tree Physiol 32:894–912.

McElrone AJ, Grant JA, Kluepfel DA (2010) The role of tyloses in crown hydraulic failure of mature walnut trees afflicted by apoplexy disorder. Tree Physiol 30:761–772.

Meyer RW, Côté WA (1968) Formation of the protective layer and its role in tylosis development. Wood Sci Technol 2:84–94.

Moore GW, Bond BJ, Jones JA, Meinzer FC (2010) Thermal-dissipation sap flow sensors may not yield consistent sap-flux estimates over multiple years. Trees 24:165–174.

Nadezhdina N, Vandegehuchte MW, Steppe K (2012) Sap flux density measurements based on the heat field deformation method. Trees 26: 1439–1448.

Oishi AC, Oren R, Novick KA, Palmroth S, Katul GG (2010) Interannual invariability of forest evapotranspiration and its consequence to water flow downstream. Ecosystems 13:421–436.

Ouellette GB (1980) Occurrence of tyloses and their ultrastructural differentiation from similarly configured structures in American elm infected by *Ceratocystis ulmi*. Can J Bot 58:1056–1073.

Parameswaran N, Knigge H, Liese W (1985) Electron microscopic demonstration of a suberised layer in the tylosis wall of beech and oak. IAWA J 6:269–271.

Parke JL, Oh E, Voelker S, Hansen EM, Buckles G, Lachenbruch B (2007) Phytophthora ramorum colonizes tanoak xylem and is associated with reduced stem water transport. Phytopathology 97:1558–1567.

Pearce RB (1991) Reaction zone relics and the dynamics of fungal spread in the xylem of woody angiosperms. Physiol and Mol Plant Pathol 39:41–56.

Pearce RB (1996) Antimicrobial defences in the wood of living trees. New Phytol 132:203–233.

Quinn GP, Keough MJ (2009) Experimental design and data analysis for biologists. Cambridge University Press, Cambridge.

Ridler TW, Calvard S (1978) Picture thresholding using an iterative selection method. IEEE Trans Syst Man Cybern 8:630–632.

Ringgaard R, Herbst M, Friborg T (2012) Partitioning of forest evapotranspiration: the impact of edge effects and canopy structure. Agric For Meteorol 166:86–97.

Rioux D, Nicole M, Simard M, Ouellette GB (1998) Immunocytochemical evidence that secretion of pectin occurs during gel (gum) and tylosis formation in trees. Phytopathology 88:494–505.

Saitoh T, Ohtani J, Fukazawa K (1993) The occurrence and morphology of tyloses and gums in the vessels of Japanese hardwoods. IAWA J 14: 359–371.

Schindelin J, Arganda-Carreras I, Frise E et al. (2012) Fiji: an open-source platform for biological-image analysis. Nat Meth 9:676–682.

Schmitt U, Liese W (1990) Wound reaction of the parenchyma in *Betula*. IAWA Bull 11:413–420.

Schmitt U, Liese W (1993) Response of xylem parenchyma by suberization in some hardwoods after mechanical injury. Trees 8:23–30.

Schwarze FWMR, Baum S (2000) Mechanisms of reaction zone penetration by decay fungi in wood of beech (*Fagus sylvatica*). New Phytologist 146:129–140.

Shibata N, Harada H, Saiki H (1981) Development and structure of traumatic tyloses in *Quercus serrata* Thunb, 1: development of traumatic tyloses in various boring seasons. JWRS J 27:618–625.

Shigo AL (1979) Tree decay an expanded concept. Agric. Inf. Bull. 419. US Department of Agriculture, Forest Service, Washington, DC, p 73.

Shigo AL (1984) Compartmentalization: a conceptual framework for understanding how trees grow and defend themselves. Annu Rev Phytopathol 22:189–214.

Shigo AL (1991) Modern arboriculture: a systems approach to the care of trees and their associates. Shigo and Trees Associates, Durham, USA.

Shortle WC, Smith KT, Dudzik KR (1996) Decay diseases of stemwood: detection, diagnosis and management. In: Raychaudhuri SP, Maramorosch K (eds). Forest trees and palms. Oxford & IBH Publishing, New Delhi, pp 95-109.

Smith DM, Allen SJ (1996) Measurement of sap flow in plant stems. J Exp Bot 47:1833–1844.

Steppe K, Cnudde V, Girard C, Lemeur R, Cnudde J-P, Jacobs P (2004) Use of X-ray computed microtomography for non-invasive determination of wood anatomical characteristics. J Struct Biol 148:11–21.

Steppe K, De Pauw DJW, Doody TM, Teskey RO (2010) A comparison of sap flux density using thermal dissipation, heat pulse velocity and heat field deformation methods. Agric For Meteorol 150: 1046–1056.

Steppe K, Vandegehuchte MW, Tognetti R, Mencuccini M (2015) Sap flow as a key trait in the understanding of plant hydraulic functioning. Tree Physiol 35:341–345.

Sun Q, Rost TL, Matthews MA (2006) Pruning-induced tylose development in stems of current-year shoots of *Vitis vinifera* (Vitaceae). Am J Bot 93:1567–1576.

Sun Q, Rost TL, Reid MS, Matthews MA (2007) Ethylene and not embolism is required for wound-induced tylose development in stems of grapevines. Plant Physiol 145:1629–1636.

Sun Q, Rost TL, Matthews MA (2008) Wound-induced vascular occlusions in *Vitis vinifera* (Vitaceae): tyloses in summer and gels in winter1. Am J Bot 95:1498–1505.

Swanson RH, Whitfield DW (1981) A numerical analysis of heat pulse velocity theory and practice. J Exp Bot 32:221–239.

Vandegehuchte MW, Steppe K (2012) Sapflow+: a four-needle heat-pulse sap flow sensor enabling nonempirical sap flux density and water content measurements. New Phytol 196:306–317.

Vandegehuchte MW, Steppe K (2013) Sap-flux density measurement methods: working principles and applicability. Funct Plant Biol 40:213–223.

Vlassenbroeck J, Dierick M, Masschaele B (2007) Software tools for quantification of X-ray microtomography at the UGCT. Nucl Instrum Methods Phys Res A 580:442–445.

Von Aufsess H (1984) Some examples of wood discolourations related to mechanisms for potential protection of living trees against fungal attack. IAWA J 5:133–138.

Wheeler EA (2011) InsideWood – a web resource for hardwood anatomy. IAWA J 32:199–211.

Wiedemann A, Marañón-Jiménez S, Rebmann C, Herbst M, Cuntz M (2016) An empirical study of the wound effect on sap flux density measured with thermal dissipation probes. Tree Physiol 36:1471–1484.

Wullschleger SD, Childs KW, King AW, Hanson PJ (2011) A model of heat transfer in sapwood and implications for sap flux density measurements using thermal dissipation probes. Tree Physiol 31:669–679.

Zimmermann MH (1979) The discovery of tyloses formation by a Viennese lady in 1845. IAWA Bull 2:51–56.